Relevance of thermal disorder in the electronic and spin ultrafast dynamics of iron in the low-perturbation regime

G. M. Pierantozzi,[1,*] A. De Vita,[1,2] R. Cucini,[1] A. M. Finardi,[1,2] T. Pincelli,[1,3] F. Sirotti,[4] J. Fujii,[1] C. Dri,[5] G. Brajnik,[5] R. Sergo,[5] G. Cautero,[5] G. Panaccione,[1,†] and G. Rossi[1,2]

[1]*Istituto Officina dei Materiali (IOM), Consiglio Nazionale delle Ricerche (CNR), in Area Science Park, S.S. 14, km 163.5, I-34149 Trieste, Italy*

[2]*Dipartimento di Fisica, Universitá degli Studi di Milano, Via Celoria 16, I-20133 Milano, Italy*

[3]*Fritz-Haber-Institut der Max-Planck-Gesellschaft, Faradayweg 4-6, Berlin 14195, Germany*

[4]*Physique de la Matiére Condensée, CNRS and École Polytechnique, Institut Polytechnique de Paris, Palaiseau 91120, France*

[5]*Elettra Sincrotrone Trieste S.C.p.A, in Area Science Park, S.S.14 - km 163.5, I-34149 Trieste, Italy*

(Received 23 May 2023; revised 18 September 2023; accepted 10 January 2024; published 13 February 2024)

Understanding the ultrafast demagnetization of transition metals requires pump-probe experiments sensitive to the time evolution of the electronic, spin, and lattice thermodynamic baths. By means of time-resolved photoelectron energy and spin-polarization measurements in the low-pump-fluence regime on iron, we disentangle the different dynamics of hot electrons and demagnetization in the subpicosecond and picosecond time range. We observe a broadening of the Fermi-Dirac distribution, following the excitation of nonthermal electrons at specific region of the iron valence band. The corresponding reduction of the spin polarization is remarkably delayed with respect to the dynamics of electronic temperature. The experimental results are corroborated with a microscopic 3-temperature model highlighting the role of thermal disorder in the quenching of the average spin magnetic moment, and indicating Elliot-Yafet type spin-flip scattering as the main mediation mechanism, with a spin-flip probability of 0.1 and a rate of energy exchange between electrons and lattice of 2.5 K fs^{-1}.

DOI: 10.1103/PhysRevB.109.064411

I. INTRODUCTION

Since the first observation of ultrafast demagnetization in a 3*d* ferromagnet following optical excitation [1], a variety of pump-probe techniques [2–9] have addressed this challenging aspect of band structure dynamics in solids. The observed phenomenology reveals (i) a demagnetization within few hundreds of femtoseconds, (ii) a partial recovery between ∼200 fs to 1 ps, and (iii) a relaxation to ground state in tens/hundreds of picoseconds. Recently, theoretical and experimental reports made increasingly clear that an explanation in the frame of a Stoner picture is insufficient [10,11] and that temperature-dependent spin fluctuations play an important role [12,13]. The statistical disorder in the spin degree of freedom can be included by using a Weiss-Heisenberg model [14] or an *ad hoc* effective temperature-dependent exchange splitting [15,16], or by introducing a band-mirroring mechanism [9,17].

In this context, it is crucial to disentangle the relevance of spin-thermal fluctuations from the contribution of electron spin redistribution in occupied and unoccupied bands [3,9] and from the direct light-spin coupling [18]. An unmediated tool for such an investigation is spin-resolved photoemission spectroscopy, only recently emerging in pump-probe experiments thanks to high-repetition-rate lasers [8,9,19,20]. In this paper, we combine two different time-resolved (TR) photoemission techniques to investigate the ultrafast response of Fe(001)-$p(1 \times 1)$O film, namely, (i) angular-resolved photoelectron spectroscopy (ARPES) to monitor changes in the electronic energy reservoir across the first Brillouin zone (fBZ) in an energy- and momentum-selective way [9,19], and (ii) spin polarization (SP) analysis of photoelectrons via Mott-scattering experiment to probe the evolution of the magnetic state [21]. We chose the Fe(001)-$p(1 \times 1)$O surface, as it is a well-characterized ferromagnetic surface and robust against contamination to ensure reproducible results in long experimental runs [22,23]. The experiments were performed in the low-perturbation regime to avoid heating the electrons above the Curie temperature and to exclude temporarily collapse of the exchange splitting [24].

We clearly distinguish the thermalized electrons from those directly excited by the pump in a specific band, observing a thermalization time ∼350 fs after the pump excitation. The dynamics of the spin polarization turns out to be markedly different with a delayed quenching. We explain the ensemble of the observations following a microscopic 3-temperature model (m-3TM) [25], which describes the heat transfer between electronic, spin, and lattice baths accounting for microscopical scattering parameters, with a Weiss-Heisenberg picture for the spin system. As a result, we identify the ultrafast demagnetization in the low-fluence regime as mainly driven by thermal fluctuations. Fit results yield a spin-flip

*Corresponding author: pierantozzi@iom.cnr.it
†Corresponding author: panaccione@iom.cnr.it

probability ∼0.1 and an electron-lattice energy exchange rate of 2.5 K fs^{-1}.

II. METHODS

The experiments were performed in the NFFA-Sprint laboratory at CNR-IOM, Trieste [26]. Measurements were conducted in ultrahigh vacuum (UHV) at a pressure $<3 \times 10^{-10}$ mbar. A 40-nm-thick Fe(001) film was grown *in situ* in a pressure $p < 2 \times 10^{-9}$ mbar epitaxially on a MgO(001) single crystal. The thickness was estimated by a quartz microbalance. A 30 min annealing at 800 K was followed by a 90 L O_2 exposure ($p = 1 \times 10^{-6}$ mbar at 450 K) and 30 s annealing at 900 K to stabilize the $p(1 \times 1)$O reconstruction [22]. The O overlayer is needed since it prevents contamination of the Fe surface for weeks in UHV. The sample is homogeneously magnetized along one in-plane easy axis, as proven by measuring vectorial SP across the sample: Hereinafter, we report only this in-plane direction. The SP values measured in two opposite azimuthal positions of the sample are used to cancel instrumental asymmetries; for TR data, the values at negative delays are employed for such rescaling.

Pulsed radiation is generated by nonlinear phenomena seeded by a pair of twin Light Conversion PHAROS lasers at 50 kHz, with 1.2 eV photon energy. To measure the SP at photothreshold, the fourth harmonic of one laser, produced by means of BBO crystals ($h\nu = 4.8$ eV, 160 fs temporal width, *s*-polarized), was used as probe beam. For ARPES spectra, we employed a photon energy of 21.7 eV from a high harmonic generation (HHG) apparatus [26], pumped by the same laser (110 fs temporal width, *s*-polarized). The other PHAROS laser feeds an optical parametric amplifier (OPA) delivering an energy-tunable pump beam (in this experiment fixed to 1.55 eV, *s*-polarized), 50 fs temporal width. The spot diameter, measured exploiting a YAG crystal at sample position, was 100 × 100 μm for the HHG beam, 550 × 300 μm for the 4.8 eV beam, and 450 ×520 μm for the pump beam.

The SP of the total photoejected electrons (i.e., integrated in k and energy) was measured with a vectorial Mott polarimeter suitable for multihit detection [27]. The sample drain current was simultaneously acquired. TR-ARPES spectra were acquired by a Scienta SES 2002 hemispherical analyzer. Additionally, static ARPES measurements were performed at the APE-LE beamline at Elettra synchrotron [23].

III. ULTRAFAST MAGNETIZATION QUENCHING

In total electron yield (TEY) mode, the contribution of secondary and inelastically scattered electrons can be minimized if photon energy slightly exceeds the sample work function (photothreshold) [28,29], thus reducing spin-filtering effects [30–32] and preserving the initial-state SP. Threshold photoelectrons are integrated over 10–15 nm of material [33] so that the contribution from the surface oxygen is negligible. The possible initial states can be identified considering conservation laws in photoemission: With $h\nu = 4.8$ eV, the signal arises from the neighborhood of E_F (<0.1 eV) and from a limited range of $k_\parallel$ (<0.2 Å^{-1}). A restriction in k_z is given by the available empty states: According to DFT calculations of bulk Fe bands at $\Gamma_\parallel$ along the Γ-H direction

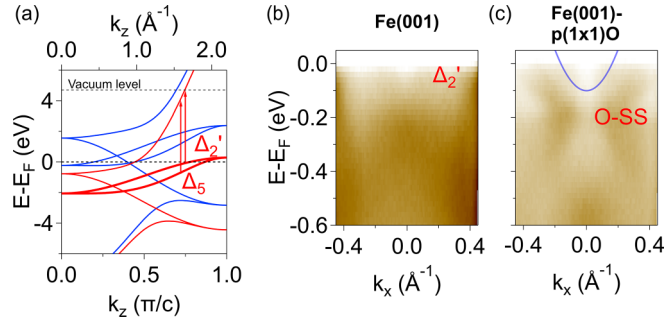

FIG. 1. (a) Density functional theory (DFT) calculations in the local density approximation (LDA) for Fe(001), showing the dispersion of the band structure at Γ as a function of k_z along the Γ-H direction. The available optical transitions to empty states close to the vacuum level for 4.8 eV are highlighted by arrows. (b) and (c) Angle-resolved photoemission spectroscopy (ARPES) spectra along the $\bar{\Gamma}$-$\bar{X}$ direction on clean Fe(001) and Fe(001)-$p(1 \times 1)$O, measured with 25 eV, *p*-polarized synchrotron radiation. The parabola encloses the maximum E-k region accessible by 4.8 eV photons according to conservation rules, given a work function of 4.7 eV.

(Fig. 1(a), in agreement with Ref. [34]), there are only two possible direct transitions of 4.8 eV toward the vacuum level, with (the majority) $\Delta_{2\uparrow}$ and $\Delta_{5\uparrow}$ bands as initial states. Both transitions lie in the range of k_z expected for photoemission at threshold ($k_{z,\mathrm{PT}} \approx 1.4$–$1.7$ Å^{-1} using inner potential values typically found in the literature [34,35]). The $\Delta_{2\uparrow}$ band can be identified in the small electronlike parabola ($k_F \approx 0.2$ Å^{-1}) observed on clean Fe(001) with $h\nu = 25$ eV [Fig. 1(b)]; at such photon energy, the corresponding k_z verifies the same condition as $k_{z,\mathrm{PT}}$ and allows us to find $\Delta_{2\uparrow}$ close to E_F at $\Gamma_\parallel$. Such a band is faintly visible also with the $p(1 \times 1)$O reconstruction [Fig. 1(c)], although it is partially covered by the more intense O surface state (O-SS) with $k_F \approx 0.35$ Å^{-1}.

The SP measured with $h\nu = 4.8$ eV is 57(5)%, in excellent agreement with early work on bulk Fe at threshold [36]. A much lower value [20(3)%] is obtained well above the threshold ($h\nu = 21.7$ eV), where the contribution of inelastic electrons dominates the TEY and averages over the full band SP. Since in both cases the SP has the same sign, the states probed by 4.8 eV must have majority character, as expected for electrons photoexcited from $\Delta_{2\uparrow}$ and $\Delta_{5\uparrow}$ bands. We can exclude any contribution to the SP from O-SS (of minority character [37]), as it lays outside the parabola in Fig. 1(c) determined by E-k conservation.

The effect of 1.55 eV pump pulses is presented in Fig. 2: In the bottom part, we observe a transient decrease of the SP, partly recovered within a few picoseconds, still partially quenched at least up to 200 ps. The quenching depends on the fluence for values not exceeding 0.3 mJ/cm^2 (Fig. 3). A phenomenological function [7,8] with the addition of a long-living exponential [5] is used to fit the SP data (as well as the TEY curve in the top of Fig. 2):

$$\left(\left\{Q\left[1-\exp\left(-\frac{t-t_0}{\tau_Q}\right)\right]\times\left[\exp\left(-\frac{t-t_0}{\tau_R}\right)+Q_S\exp\left(-\frac{t-t_0}{\tau_S}\right)\right]\right\}\Theta(t,t_0)\right), \quad (1)$$

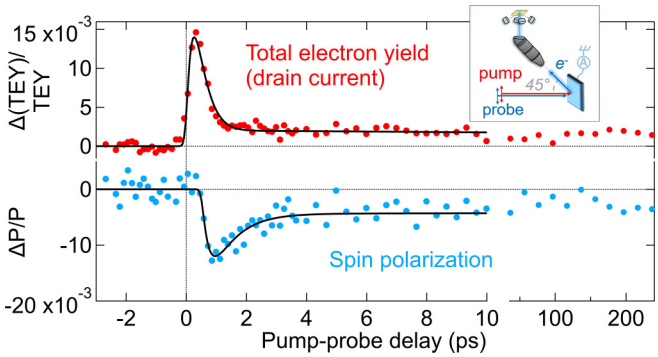

FIG. 2. Time-resolved relative variation of total electron yield (TEY; top) and spin polarization (SP; bottom) at 1.3 mJ/cm^2 pump fluence, using 4.8 eV probe and 1.55 eV pump. Inset: Experimental geometry.

where τ_Q is the quenching time constant, and τ_R and τ_S describe, respectively, the fast and slow recoveries (the latter fixed at 200 ps). The function is convoluted with a Gaussian accounting for the temporal resolution (fixed at 160 fs). For the investigated fluences (see Table I), τ_Q and τ_R are in good agreement with ultrafast demagnetization measurements at higher fluences, employing the magneto-optical Kerr effect on *3d* transition metals [1,24,25,38] and specifically on Fe(001) on MgO(001) [5] or W(110) [7]. Our observation of a long-living demagnetized state is in contrast with the results of Tengdin *et al.* [24], who observed a slow-decaying tail only above the exchange splitting collapse threshold. We argue that the tail is linked to the heat diffusion, which takes hundreds of picoseconds to relax [5,39].

Additional information can be gained through the TEY curve in the top of Fig. 2. Given the low photon energy, the peak and the following relaxation trend in this curve can be attributed to the broadening of the electron distribution after the pump pulse. The TEY increase precedes the SP decrease, and the TEY fast relaxation time (<300 fs) is significantly smaller than τ_R. Given such differences with the electronic distribution evolution simultaneously measured, the observed SP behavior cannot be explained by the redistribution of spin-polarized

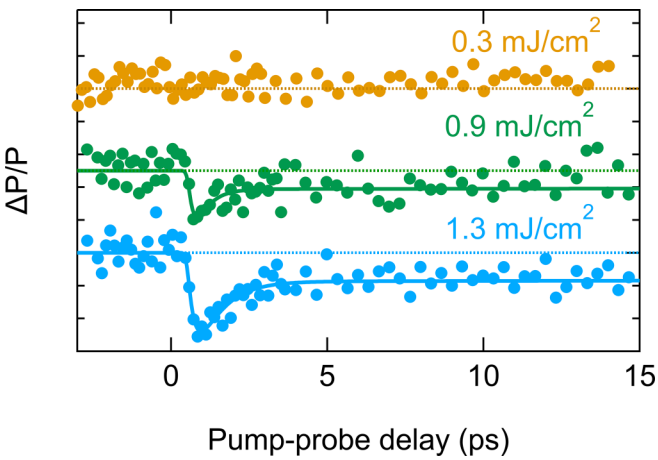

FIG. 3. Time-resolved relative variation of spin polarization (SP) as a function of pump fluence.

TABLE I. Fit results of the SP dynamics.

Pulse energy (μJ)	Fluence (mJ/cm^2)	Q	τ_Q (fs)	τ_R (fs)
3.4	1.3	2.0%	290 ± 136	772 ± 138
2.3	0.9	1.3%	202 ± 82	436 ± 96

carriers close to E_F, as proposed in previous experiments on Co [9] and Fe [20]. We also exclude superdiffusive spin currents [9] due to the insulating substrate and the long τ_Q. We thus propose that the observed SP reduction is an effect of the quenching of the magnetic moment due to an increase of thermal disorder in the spin degree of freedom after the absorption of optical energy by the electrons. This picture is in agreement with recent theoretical findings on the parameters governing the ultrafast demagnetization [12].

IV. ULTRAFAST DYNAMICS OF ELECTRONS

We now accurately address the induced changes in the electronic distribution over the whole BZ, by means of ARPES with $h\nu = 21.7$ eV as probe (same 1.55 eV pump at 1.3 mJ/cm^2 at normal incidence) imaging the whole BZ by rotating the polar angle, with light polarization parallel to the rotation axis [Fig. 4(a)]. Static ARPES measurements on $p(1 \times 1)$O-Fe(001) are presented in Fig. 4(b). Well-known O-induced states are located in the range from 4 to 6 eV binding energy (BE) [40,41]. Close to E_F, we observe contributions from both bulk Fe and the O overlayer (see Supplemental Material, Fig. S5 [42]).

TR-ARPES measurements have been carried out in three regions of the BZ [colored rectangles in Fig. 4(b)], displayed in Figs. 4(c)–4(e), corresponding to incidence angles, respectively, of 15°, 34°, and 65°, with effective fluence scaling accordingly. The sharp band in Fig. 4(f) is visible up to 0.4 eV above E_F in the pumped state at t_0 and almost disappearing after 300–500 fs. The integration over the selected k region [displayed in Fig. 4(f)] shows that the fastest intensity rise occurs in the range 0.4–0.8 eV above E_F (gold-green curves), recovering to the equilibrium state within the pump-pulse duration. The energy scale and the temporal behavior of such transient state—not observed in the other regions of the BZ—cannot be explained by a broadening of the Fermi-Dirac distribution, hinting at a nonthermal nature [43,44]. Some tens of femtoseconds later, a peak is also reached at lower energy, within 0.2 eV above E_F (black curve), with a concomitant decrease just below E_F (red curve), followed by a partial relaxation within 0.5 ps and by a long-living tail (see also Supplemental Material, Fig. S2 [42]). This behavior is compatible with a broadening of the Fermi step due to a temperature increase of the electron population, resulting from e-e scattering after the excitation of nonthermal electrons; the fast relaxation is due to thermalization with phonons [45]. The latter kind of trend is mirrored in the other regions of the BZ [Fig. 4(g)], confirming its thermal nature and the negligible dependence on the specific bands crossing Fermi level as well as on the fluence (due to different incidence angles) within our low perturbation regime. We stress that such

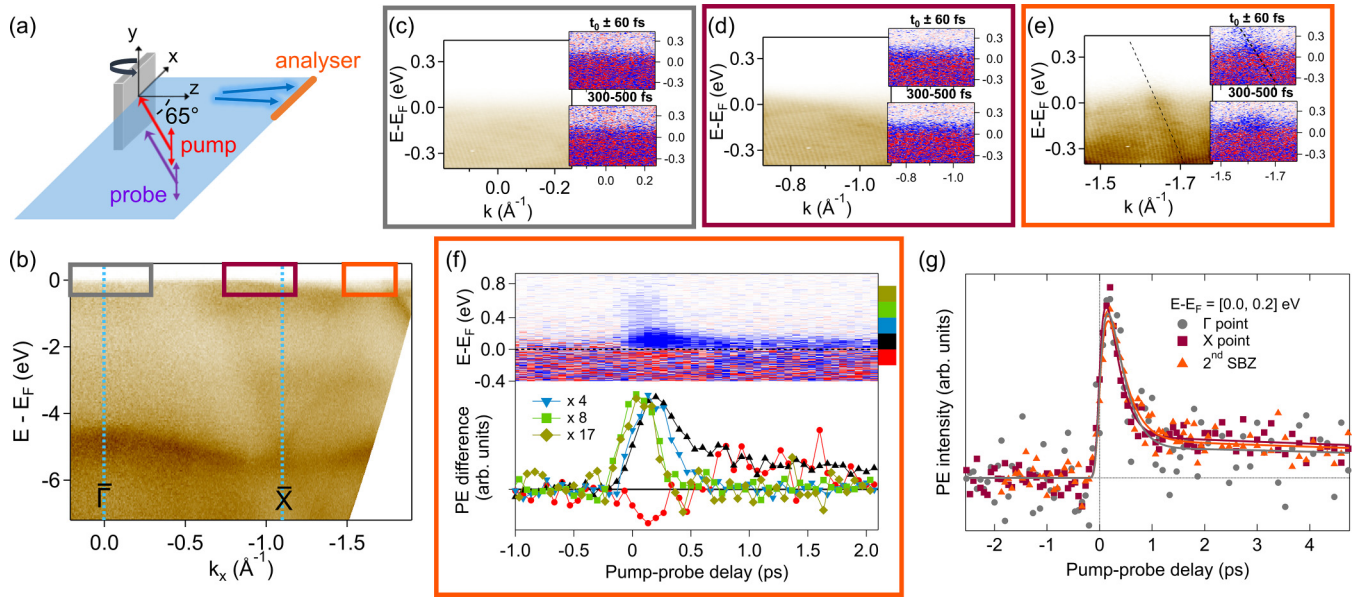

FIG. 4. (a) Cartoon representation of the time-resolved (TR) angle-resolved photoemission spectroscopy (ARPES) experimental geometry. (b) ARPES static measurement at 21.7 eV, s-polarized. (c)–(e) TR-ARPES with 1.55 eV pump and 21.7 eV probe, measured in the regions of (b) highlighted by the colored rectangles. Main panel: Spectrum averaged over the temporal delays before t_0. Insets: In the top (bottom), the difference between the spectrum at $t_0 \pm 60$ fs (300–500 fs) and the average before t_0 (blue positive, red negative). (f) k-integrated spectrum of (e) vs delay. Top: Difference map after subtraction of the average before t_0 (blue positive, red negative). Bottom: Delay cuts in the energy ranges indicated by the colored rods in the top panel, multiplied by arbitrary factors to compare their line shapes. (g) Comparison of the behavior of thermal electrons in the three regions of momentum space highlighted in (b), with corresponding colors: The intensity difference integrated from 0–0.2 eV is rescaled to compensate different photoemission intensities due to pump fluence dependence on the incidence angle.

behavior of the electronic distribution around the Fermi level is also independent of the coherent size of the $p(1 \times 1)$O domains (see Supplemental Material, Fig. S6 [42]). Exploiting the fitting function in Eq. (1) (temporal width fixed to 110 fs), the thermalization time results 350(50) fs, in agreement with results on Fe/W(110) [19] and Co/Cu(001) [3], and the fast relaxation time 235(25) fs. Consistent results have been obtained with p-polarized probe and different pump energy (see Supplemental Material, respectively, Figs. S3 and S4 [42]).

Since nonthermal electrons are observed only at $k_F = 1.65\,\text{Å}^{-1}$, in the other regions, we can describe the electron system using a time-dependent Fermi-Dirac distribution (FDD) at each pump-probe delay. The thermal process can be disentangled from the spectral function by means of the procedure described by Buhlmann *et al.* [20], which yields a function to be fitted with the FDD $f_{\text{FD}}(E;\mu,T_e) = \{1+\exp[-(E-\mu)/kT_e]\}^{-1}$ convoluted with an experimental Gaussian broadening, with chemical potential μ and electronic temperature T_e as free parameters. The former does not change within 1 meV, well below our energy resolution. The extracted T_e is displayed in Fig. 5 as a function of the delay for measurements at $\bar{\text{X}}$ (top, red dots), increasing up to 360 K (well below the Curie temperature) within few hundreds of femtoseconds, and then recovering to a value slightly above equilibrium. The small increase justifies *a posteriori* the assumption of a constant spectral function, i.e., no modifications in the band structure and especially in the exchange splitting, as expected for a maximum quenching of 1%.

V. DISCUSSION

To describe the heat transfer among different degrees of freedom, we employ the m-3TM by Koopmans *et al.* [25], where the microscopic mechanism of phonon-mediated Elliot-Yafet spin-flip scattering is implemented in the temporal evolution of the spin system, treated with a Heisenberg Hamiltonian in the mean-field Weiss approximation. Here,

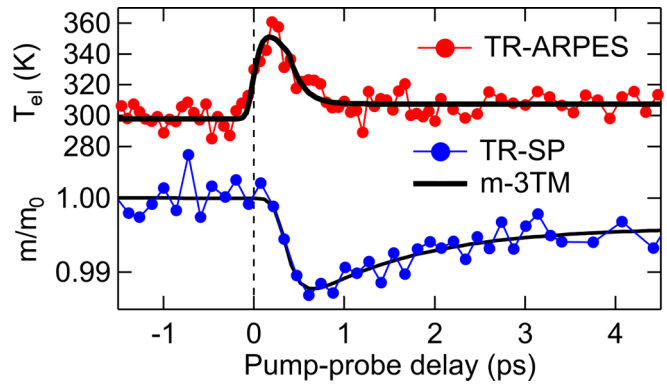

FIG. 5. Electronic temperature [top, from the time-resolved (TR) angle-resolved photoemission spectroscopy (ARPES) experiment] and relative magnetic moment [bottom, from the TR spin-polarization (SP) experiment]. Black lines are fits based on the microscopic 3-temperature model (m-3TM). The temporal alignment has been retrieved using t_0 values obtained by the two independent fit procedures.

TABLE II. Fit results according to the m-3TM.

Fitted curves	g_{ep} 10^{18} J (sm^3 K)$^{-1}$	R ps^{-1}
$T_e(t)$, X point	1.5(1)	2.5(5)
$m(t)$, 1.3 mJ/cm^2	1.8(2)	2.5(4)
$m(t)$, 0.9 mJ/cm^2	1.7(3)	2.5(7)

we suppose that the measured SP is related to the average magnetic moment m, based on the discussion of Fig. 2. Additionally, following Carpene *et al.* [43], we add the nonthermal contributions $\partial U_{ee}/\partial t$ and $\partial U_{ep}/\partial t$ to the electronic (T_e) and lattice (T_p) differential equations, respectively; such terms describe the energy transfer from nonthermal electrons to thermal electrons and lattice, thus accounting for the slower thermalization compared to the laser pulse duration. This is modeled as a Gaussian profile, with temporal width fixed to 110 fs for T_e and 160 fs for m, and included in $\partial U_{ee}/\partial t$ and $\partial U_{ep}/\partial t$. No additional term is needed in the differential equation for m since the spin dynamics results are unaffected by the presence of nonthermal electrons within our resolution. The equations read

$$\gamma_e T_e \frac{dT_e}{dt} = -g_{ep}(T_e - T_p) + \frac{\partial U_{ee}}{\partial t}, \tag{2}$$

$$C_p \frac{dT_p}{dt} = -g_{ep}(T_p - T_e) - k(T_p - T_0) + \frac{\partial U_{ep}}{\partial t}, \tag{3}$$

$$\frac{dm}{dt} = Rm\frac{T_p}{T_C}\left(1 - m\coth\frac{mT_C}{T_e}\right). \tag{4}$$

The lattice specific heat C_p is assumed independent of temperature ($C_p = 3.527$ J/cm^3 K) and the electronic specific heat as proportional to T_e through the factor $\gamma_e = 0.7$ mJ/cm^3 K^2 [46]. The fit parameters are the electron-phonon coupling g_{ep} and the scaling factor R:

$$R = \frac{8a_{sf}g_{ep}k_B T_C^2 V_{at}}{(\mu_{at}/\mu_B)E_D^2}, \tag{5}$$

where $a_{\rm sf}$ is the spin-flip scattering probability, T_C the Curie temperature [1043 K], $V_{\rm at}$ the atomic volume [11.8 Å^3], μ_{at}/μ_B the atomic magnetic moment in units of Bohr magneton [2.2], E_D the Debye energy [0.04 eV] and k_B the Boltzmann constant.

The fits of T_e and m curves according to the m-3TM have been performed independently, with consistent results (see Table II) and excellent agreement with data, as displayed in Fig. 5. By averaging the parameters in Table II and solving for a_{sf} in Eq. (5), we find $a_{sf} = 0.104(29)$, in line with values in the literature for Ni and Co [25]. The resulting g_{ep} gives a good estimation of the rate for energy exchange between electrons and lattice $g_{ep}/\gamma_e = 2.5$ K/fs, where the order of magnitude for most metals is ∼1 K/fs [47].

The good agreement with a model in which the magnetic moment variation intrinsically has a thermal and collective origin (Weiss-Heisenberg picture) supports the interpretation of SP at the Fermi level in iron as reflecting the behavior of the average magnetic moment. The delayed dynamics of the spin degree of freedom observed here in the low-perturbation regime is well accounted by this model: The average magnetic moment starts changing only when the electrons have thermalized. The partial recovery of the magnetic moment within a few picoseconds reflects the complete thermalization of the three different baths.

VI. CONCLUSIONS

In conclusion, the electronic temperature and the magnetic moment at E_F after moderate optical excitation behave differently within 2–3 ps: The SP quenches only after the electron gas is fully heated and the thermalization with the lattice is activated and then recovers with a larger time constant with respect to T_e. On the other hand, the trends of the long-living tail up to hundreds of picoseconds show a clear correspondence, a signature of the thermalization of the three reservoirs. Our results demonstrate that, in the low-fluence regime, the transient spin variation is due to thermal fluctuations, driven by the increase of the electronic temperature upon pump excitation, once nonthermal electrons have transferred their excess energy to the whole electron bath.

ACKNOWLEDGMENTS

This paper has been performed in the framework of the Nanoscience Foundry and Fine Analysis (NFFA-MUR Italy Progetti Internazionali) facility. Thanks are due to D. M. Janas, M. Cinchetti, and C. H. Back for useful suggestions and discussion, and to A. Fondacaro and D. Krizmancic for technical support.

G.M.P. and A.D.V. contributed equally to this paper.

[1] E. Beaurepaire, J.-C. Merle, A. Daunois, and J.-Y. Bigot, Phys. Rev. Lett. **76**, 4250 (1996).

[2] J. Güdde, U. Conrad, V. Jähnke, J. Hohlfeld, and E. Matthias, Phys. Rev. B **59**, R6608 (1999).

[3] M. Cinchetti, M. S. Albaneda, D. Hoffmann, T. Roth, J.-P. Wüstenberg, M. Krauß, O. Andreyev, H. C. Schneider, M. Bauer, and M. Aeschlimann, Phys. Rev. Lett. **97**, 177201 (2006).

[4] C. Stamm, T. Kachel, N. Pontius, R. Mitzner, T. Quast, K. Holldack, S. Khan, C. Lupulescu, E. F. Aziz, M. Wietstruk *et al.*, Nat. Mater. **6**, 740 (2007).

[5] E. Carpene, E. Mancini, C. Dallera, M. Brenna, E. Puppin, and S. De Silvestri, Phys. Rev. B **78**, 174422 (2008).

[6] C. La-O-Vorakiat, M. Siemens, M. M. Murnane, H. C. Kapteyn, S. Mathias, M. Aeschlimann, P. Grychtol, R. Adam, C. M. Schneider, J. M. Shaw *et al.*, Phys. Rev. Lett. **103**, 257402 (2009).

[7] A. Weber, F. Pressacco, S. Günther, E. Mancini, P. M. Oppeneer, and C. H. Back, Phys. Rev. B **84**, 132412 (2011).

[8] A. Fognini, T. U. Michlmayr, G. Salvatella, C. Wetli, U. Ramsperger, T. Bähler, F. Sorgenfrei, M. Beye, A.

Eschenlohr, N. Pontius *et al.*, Appl. Phys. Lett. **104**, 032402 (2014).
[9] S. Eich, M. Plötzing, M. Rollinger, S. Emmerich, R. Adam, C. Chen, H. C. Kapteyn, M. M. Murnane, L. Plucinski, D. Steil *et al.*, Sci. Adv. **3**, e1602094 (2017).
[10] E. Carpene, H. Hedayat, F. Boschini, and C. Dallera, Phys. Rev. B **91**, 174414 (2015).
[11] E. Turgut, D. Zusin, D. Legut, K. Carva, R. Knut, J. M. Shaw, C. Chen, Z. Tao, H. T. Nembach, T. J. Silva *et al.*, Phys. Rev. B **94**, 220408(R) (2016).
[12] Z. Chen and L.-W. Wang, Sci. Adv. **5**, eaau8000 (2019).
[13] J. Minár, S. Mankovsky, J. Braun, and H. Ebert, Phys. Rev. B **102**, 035107 (2020).
[14] A. J. Schellekens and B. Koopmans, Phys. Rev. Lett. **110**, 217204 (2013).
[15] B. Y. Mueller, A. Baral, S. Vollmar, M. Cinchetti, M. Aeschlimann, H. C. Schneider, and B. Rethfeld, Phys. Rev. Lett. **111**, 167204 (2013).
[16] A. L. Chekhov, Y. Behovits, J. J. F. Heitz, C. Denker, D. A. Reiss, M. Wolf, M. Weinelt, P. W. Brouwer, M. Münzenberg, and T. Kampfrath, Phys. Rev. X **11**, 041055 (2021).
[17] B. Andres and M. Weinelt, J. Magn. Magn. Mater. **501**, 166475 (2020).
[18] J.-Y. Bigot, M. Vomir, and E. Beaurepaire, Nat. Phys. **5**, 515 (2009).
[19] R. Gort, K. Bühlmann, S. Däster, G. Salvatella, N. Hartmann, Y. Zemp, S. Holenstein, C. Stieger, A. Fognini, T. U. Michlmayr *et al.*, Phys. Rev. Lett. **121**, 087206 (2018).
[20] K. Bühlmann, G. Saerens, A. Vaterlaus, and Y. Acremann, Struct. Dyn. **7**, 065101 (2020).
[21] T. J. Gay and F. B. Dunning, Rev. Sci. Instrum. **63**, 1635 (1992).
[22] R. Bertacco and F. Ciccacci, Phys. Rev. B **59**, 4207 (1999).
[23] C. Bigi, P. K. Das, D. Benedetti, F. Salvador, D. Krizmancic, R. Sergo, A. Martin, G. Panaccione, G. Rossi, J. Fujii *et al.*, J. Synchrotron Radiat. **24**, 750 (2017).
[24] P. Tengdin, W. You, C. Chen, X. Shi, D. Zusin, Y. Zhang, C. Gentry, A. Blonsky, M. Keller, P. M. Oppeneer *et al.*, Sci. Adv. **4**, eaap9744 (2018).
[25] B. Koopmans, G. Malinowski, F. D. Longa, D. Steiauf, M. Fähnle, T. Roth, M. Cinchetti, and M. Aeschlimann, Nat. Mater. **9**, 259 (2010).
[26] R. Cucini, T. Pincelli, G. Panaccione, D. Kopic, F. Frassetto, P. Miotti, G. M. Pierantozzi, S. Peli, A. Fondacaro, A. De Luisa *et al.*, Struct. Dyn. **7**, 014303 (2020).
[27] T. Pincelli, V. N. Petrov, G. Brajnik, R. Ciprian, V. Lollobrigida, P. Torelli, D. Krizmancic, F. Salvador, A. De Luisa, R. Sergo *et al.*, Rev. Sci. Instrum. **87**, 035111 (2016).
[28] H. E. Farnsworth, Phys. Rev. **27**, 413 (1926).
[29] A. Bellissimo, G. M. Pierantozzi, A. Ruocco, G. Stefani, O. Y. Ridzel, V. Astašauskas, W. S. M. Werner, and M. Taborelli, J. Electron Spectrosc. Relat. Phenom. **241**, 146883 (2020).
[30] E. Kisker, W. Gudat, and K. Schröder, Solid State Commun. **44**, 591 (1982).
[31] H. Hopster, R. Raue, E. Kisker, G. Güntherodt, and M. Campagna, Phys. Rev. Lett. **50**, 70 (1983).
[32] M. Aeschlimann, M. Bauer, S. Pawlik, W. Weber, R. Burgermeister, D. Oberli, and H. C. Siegmann, Phys. Rev. Lett. **79**, 5158 (1997).
[33] G. K. L. Marx, P.-O. Jubert, A. Bischof, and R. Allenspach, Appl. Phys. Lett. **83**, 2925 (2003).
[34] E. Młyńczak, M. Eschbach, S. Borek, J. Minár, J. Braun, I. Aguilera, G. Bihlmayer, S. Döring, M. Gehlmann, P. Gospodarič *et al.*, Phys. Rev. X **6**, 041048 (2016).
[35] E. Młyńczak, I. Aguilera, P. Gospodarič, T. Heider, M. Jugovac, G. Zamborlini, C. Tusche, S. Suga, V. Feyer, S. Blügel *et al.*, Phys. Rev. B **103**, 035134 (2021).
[36] W. Eib and B. Reihl, Phys. Rev. Lett. **40**, 1674 (1978).
[37] A. M. Finardi, All-resolved photoemission spectroscopy of Fe(100) and passivated Fe-$p(1 \times 1)$O surfaces, Bachelor's Thesis, University of Milan, 2020.
[38] A. J. Schellekens, W. Verhoeven, T. N. Vader, and B. Koopmans, Appl. Phys. Lett. **102**, 252408 (2013).
[39] T. Pincelli, R. Cucini, A. Verna, F. Borgatti, M. Oura, K. Tamasaku, H. Osawa, T.-L. Lee, C. Schlueter, S. Günther *et al.*, Phys. Rev. B **100**, 045118 (2019).
[40] G. Panzner, D. R. Mueller, and T. N. Rhodin, Phys. Rev. B **32**, 3472 (1985).
[41] D. M. Janas, A. Droghetti, S. Ponzoni, I. Cojocariu, M. Jugovac, V. Feyer, M. M. Radonjić, I. Rungger, L. Chioncel, G. Zamborlini *et al.*, Adv. Mater. **35**, 2205698 (2023).
[42] See Supplemental Material at http://link.aps.org/supplemental/10.1103/PhysRevB.109.064411 for static spin polarization; electron dynamics at long delays; probe polarization dependence of electron dynamics; pump energy dependence of electron dynamics; robustness of electron dynamics against surface inhomogeneity.
[43] E. Carpene, Phys. Rev. B **74**, 024301 (2006).
[44] M. Uehlein, S. T. Weber, and B. Rethfeld, Nanomaterials **12**, 1655 (2022).
[45] N. Del Fatti, C. Voisin, M. Achermann, S. Tzortzakis, D. Christofilos, and F. Vallée, Phys. Rev. B **61**, 16956 (2000).
[46] L. Kaufman, E. Clougherty, and R. Weiss, Acta Metall. **11**, 323 (1963).
[47] G. Ferrini, F. Banfi, C. Giannetti, and F. Parmigiani, Nucl. Instrum. Methods Phys. Res. Sect. A **601**, 123 (2009).